

Voltage-dependent conductance of a single graphene nanoribbon

Matthias Koch¹, Francisco Ample², Christian Joachim^{2,3} and Leonhard Grill^{1*}

Graphene nanoribbons could potentially be used to create molecular wires with tailored conductance properties. However, understanding charge transport through a single molecule requires length-dependent conductance measurements and a systematic variation of the electrode potentials relative to the electronic states of the molecule^{1,2}. Here, we show that the conductance properties of a single molecule can be correlated with its electronic states. Using a scanning tunnelling microscope, the electronic structure of a long and narrow graphene nanoribbon, which is adsorbed on a Au(111) surface, is spatially mapped and its conductance then measured by lifting the molecule off the surface with the tip of the microscope. The tunnelling decay length is measured over a wide range of bias voltages, from the localized Tamm states over the gap up to the delocalized occupied and unoccupied electronic states of the nanoribbon. We also show how the conductance depends on the precise atomic structure and bending of the molecule in the junction, illustrating the importance of the edge states and a planar geometry.

Electron transport through a long molecule, which is fundamental in chemical and biological processes³, depends on the electronic structure of the molecule, its interaction with the junction electrodes and the energy position of the molecular electronic states with respect to the electrodes⁴. The relation between the molecular electronic structure and the exponential decay of electron transfer rate with length has been studied experimentally in solution⁵. Several groups have also investigated charge transport for various lengths of molecular wires when contacting their termini to electrodes, either by comparing different molecules^{1,6–8} or by continuously changing the electrode distance along the molecule^{9,10}. In one study¹¹, the bias voltages of the electrodes were varied, but the electron energy always remained at low voltages in the gap between the ground state (that is, the highest occupied molecular orbital, HOMO) and the first excited states (that is, the lowest unoccupied molecular orbital, LUMO) of the molecular wire, while several thousands of molecules were present in the junction at the same time. However, measurements at the level of a single and well-characterized molecule^{9,10} are necessary, because the conductance per molecule in an ensemble can differ significantly from that of an individual molecule¹².

The conductance of a molecular wire (length, d) follows the well-known $G(d) = G_0 e^{-\beta d}$ exponential decay, where G_0 is the contact conductance and β is the inverse decay length through the wire¹⁰. The latter depends on the position of the HOMO and LUMO relative to the Fermi level E_F , their energy difference E_g , and the effective mass of the electron in the tunnelling junction¹³. A large E_g leads to a high β value and consequently to a low junction conductance, for example for alkane chains¹⁴. Another transport regime is active if the molecule in the junction exhibits electronic states that are located at E_F . In such a case, β becomes very small, such as with

the d states of an organometallic compound⁸ or the π states of a short organic molecular wire¹⁵. Consequently, a pseudo-ballistic transport regime with $G < 2e^2/h$ (that is, the quantum of conductance) results, because the electronic structure of the molecular wire differs from that of the metallic electrodes. Here, we are interested in a third transport regime where the electronic structure of the molecular wire is designed to keep β as small as possible while maintaining a non-zero E_g , which can be realized by achieving a rather small effective mass. Such a tunnelling transport represents an interesting regime, because it can be tuned via the electronic states of the molecule supporting the tunnelling regime in the gap, even at a fixed E_g value¹⁶.

Narrow graphene nanoribbons were studied on Au(111) because their electronic structure can be controlled via their width¹⁷ and edge structure¹⁸ (zigzag or armchair). In contrast to top-down approaches^{19–21}, which lack control over the ribbon width and/or edge structure at the atomic scale, bottom-up on-surface polymerization²² produces precisely defined molecular structures. This level of precision is required for charge transport studies as structural defects modify the electronic structure and reduce the conductance²³. We used 10,10'-dibromo-9,9'-bianthryl molecules (Fig. 1a) to produce graphene nanoribbons with an armchair edge structure²⁴. After on-surface polymerization at 200 °C, during which non-planar anthracene oligomers were formed (Fig. 1b), a second heating step at 400 °C led to cyclodehydrogenation (Fig. 1c). All experiments were carried out under ultrahigh vacuum conditions by scanning tunnelling microscopy (STM) at temperatures of ~ 10 K (see Methods). The graphene nanoribbons appear as straight stripes with an apparent height of 1.85 ± 0.12 Å. Their contour is rather homogeneous, but they exhibit characteristic finger-like lobes at both termini (Fig. 1d), independent of the ribbon length, if small bias voltages are used (Supplementary Fig. S1). These features are typical for the intact molecule if the bromine atoms are already dissociated, whereas other appearances are observed with chemically different termini (Supplementary Fig. S2).

To study the electronic origin of the bias-dependent appearance, dI/dV spectra, which are known to reflect the electronic transparency of the junction²⁵, were recorded as a function of voltage. Typical spectra of the molecular termini exhibit a peak at ~ 30 meV above the Fermi level, which strongly depends on the tip position over the molecule: while it is pronounced at the two termini, it completely vanishes at the centre (Fig. 1d,e). In addition to the edge lengths (narrow at the termini and long on the side), the main difference between these two areas lies in the structure of the ribbon edge, which is zigzag at the termini and armchair sideways. We assign the peak observed at the Fermi level (as mentioned above) to Tamm states²⁶, which originate from the specific arrangement of carbon atoms at the zigzag edges and are absent at armchair edges, in agreement with our observations (similar spectra are detected along the central ribbon axis; Supplementary Fig. S9). These Tamm states

¹Department of Physical Chemistry, Fritz-Haber-Institute of the Max-Planck-Society, 14195 Berlin, Germany, ²Institute of Materials Research and Engineering (IMRE), 117602 Singapore, ³Nanosciences Group and MANA Satellite, CEMES-CNRS, 31055 Toulouse, France. *e-mail: lgr@fhi-berlin.mpg.de

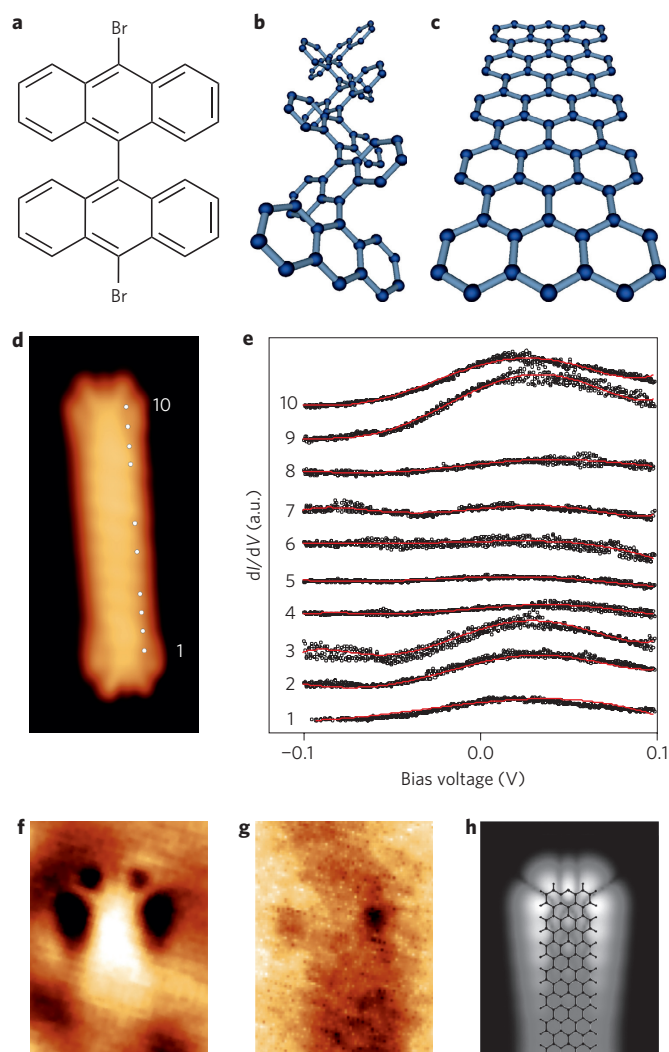


Figure 1 | Electronic structure of single graphene nanoribbons. **a–c**, Chemical structure of the 10,10'-dibromo-9,9'-bianthryl molecules (**a**), which are connected to oligomers (**b**; calculated gas phase structure) in the first heating step and to graphene nanoribbons (**c**) in the second heating step. **d,e**, STM image ($3 \times 7 \text{ nm}^2$) (**d**) and corresponding dI/dV curves (**e**) taken at different positions (1–10) along a single nanoribbon, revealing the presence of a peak at the ribbon termini that decays within $\sim 10\text{--}15 \text{ \AA}$ along the ribbon. **f–h**, Conductance maps of the same molecule at bias voltages of 0.05 V (**f**) and -0.55 V (**g**) and a calculated ESQC (elastic scattering quantum chemistry) conductance map (**h**), calculated at 50 mV bias voltage (all $3 \times 4 \text{ nm}^2$). The chemical structure is superimposed in **h**.

have been predicted theoretically²⁷ and observed for the first time very recently at kinked ribbon edges²⁸. The precise chemical edge structure plays an important role as we observe no Tamm states in the experiments for any other nanoribbon terminus with a defect, a bromine substituent atom or for anthracene oligomers (Supplementary Fig. S3). The localization of each Tamm state at the terminus was illustrated by mapping their spatial distribution (Fig. 1f), which was found to be in agreement with a calculated conductance map (Fig. 1h). Note that the same area turned out to be featureless when a slightly different bias voltage was used in the experiment (that is, in the gap between HOMO and Tamm state; Fig. 1g).

For conductance measurements, a single graphene nanoribbon was lifted off the surface by controlled pulling using an STM^{9,10}, attaching one end to the tip then characterizing it before and afterwards by imaging and spectroscopy. During tip retraction, the effective transport length through the ribbon (indicated by an

arrow in Fig. 2a) was modified, because the current passes only through the part of the nanoribbon that does not interact with the surface¹⁰. A successful molecule attachment can be identified from the STM current signal $I(z)$ during the pulling sequence, as it results in a smaller slope (that is, higher conductance) than for the vacuum junction. From the linear curves in the logarithmic plot (therefore exponential decay, Fig. 2b), we found that electron transport always occurs in the tunnelling regime, with different slopes for different bias voltages. However, the steepest curve (and therefore a rather large β value of $0.76 \pm 0.04 \text{ \AA}^{-1}$) is found for the anthracene oligomer (Fig. 2b; taken at a bias voltage of 50 mV), that is, for the same molecules before planarization (Fig. 1b), because of their lower electron delocalization and larger E_g value. Note that all pulling curves in Fig. 2b are very smooth, in contrast to the local bending of a chain-like polyfluorene, which causes characteristic oscillations in the current curve¹⁰. These constant slopes point to a continuous bending of the ribbon in the junction, which is confirmed by calculations (Fig. 2c, Supplementary Fig. S4). Note that although the interaction of the planar aromatic board with the metal is significant, lateral displacement of the ribbon (even over lengths of 20 nm) on the surface occurs as a consequence of the pulling procedure. The laterally shifted ribbon maintains its perfectly linear shape on the surface (Fig. 2d,e) due to its mechanical stiffness.

When systematically measuring pulling curves for different bias voltages (that is, with the electrode electron energies shifted with respect to the graphene nanoribbon), quite different slopes are obtained (Fig. 2b), with a characteristic decay constant for each bias voltage. Specifically, the curves are steeper and the slope rather high at small bias voltages. However, the slopes tend to decrease and, accordingly, the conductance rises when moving to higher bias values. To understand these changes in conductance, dI/dV spectra of a single nanoribbon were measured (Fig. 3a) in a pulling geometry. Two peaks at -1.1 V and 1.6 V were found, which arise from the HOMO and LUMO of the molecule (dI/dV maps at these energies are presented in Supplementary Fig. S5), indicating $E_g = 2.7 \text{ eV}$. To correlate these values to the charge transport mechanisms, $I(z)$ measurements were carried out for bias voltages between -1.8 V and $+2.4 \text{ V}$, hence covering all relevant electronic states (HOMO, LUMO and Tamm states). From the exponential decay of the current with tip height, which was observed for all voltages (as in Fig. 2b), the inverse decay length β was determined as a function of bias voltage (Fig. 3b). Note that the slope remains the same for different ribbon lengths in repeated attempts with a single ribbon, and is not modified by the presence of a defect at the terminus (Supplementary Figs S10, S12 and S13). Three plateaux can be distinguished. At low bias voltages (up to $\sim 1.6 \text{ V}$), β values around $0.45 \pm 0.06 \text{ \AA}^{-1}$ are found. In a tunnelling transport regime, the decay depends on the electron energy, the molecular energy levels (E_h and E_l are the positions of HOMO and LUMO, respectively) and the effective mass m^* of the electrons¹³

$$\beta(E) = \sqrt{\frac{2m^*(E)(E - E_h)(E_l - E)}{\hbar^2 E_g}} \quad (1)$$

β is therefore expected to decrease as soon as the electron energy matches a molecular energy level. This behaviour can be seen in Fig. 3a,b, where the onsets of the changes in β (at -1.3 eV and $+1.6 \text{ eV}$) coincide with the positions of the molecular electronic resonances in the dI/dV spectrum (at -1.1 eV and $+1.6 \text{ eV}$, respectively), resulting in lower β values of $0.18 \pm 0.03 \text{ \AA}^{-1}$ (at $1.8\text{--}2.4 \text{ V}$) and a continuous reduction down to $\sim 0.1 \text{ \AA}^{-1}$ at negative bias voltages. This is in qualitative agreement with calculations (Fig. 3c,d), as the decrease in β value matches the onset of the delocalized HOMO and LUMO molecular orbitals. Our calculations

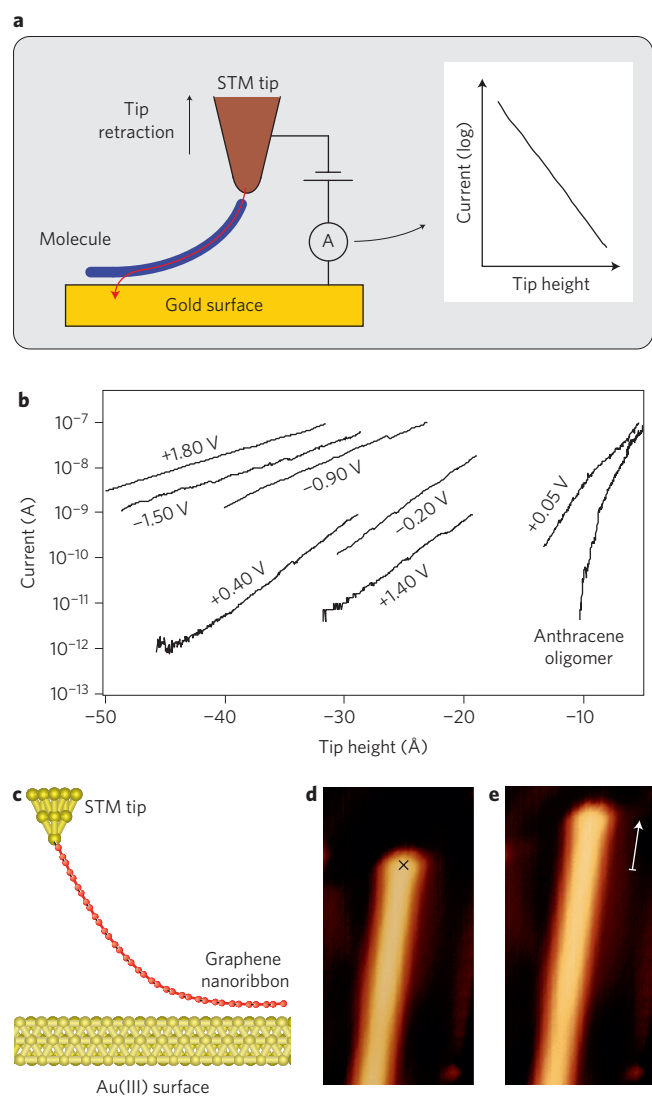


Figure 2 | Single-molecule conductance measurements. **a**, Schematic of the STM pulling experiment (arrow indicates tunnelling current). A characteristic current signal during the pulling sequence is shown in the right panel. **b**, Current as a function of tip height for different experiments (zero tip height refers to tip-surface contact). For complete curves see Supplementary Fig. S6. Different ribbon lengths were used in the experiments, resulting in equivalent conductance properties (see Supplementary Information). **c**, Calculated nanoribbon configuration in the junction during a pulling sequence. **d,e**, STM images ($14 \times 7 \text{ nm}^2$) of the same surface area before (**d**) and after (**e**) a pulling procedure reveal the lateral displacement on the surface (indicated by arrow) with respect to a fixed defect (lower right corner).

show that the asymmetry in the inverse decay length at positive and negative bias voltages is due to the asymmetric distribution of the electronic states, while a symmetric distribution around the Fermi level leads to a symmetric β curve. Moreover, increased β values are measured at energies very close to the Fermi level (Fig. 3b), as well as for ribbons that have a defect and thus no Tamm state at their termini (Supplementary Fig. S12). This peak seems to originate from the bending of the nanoribbon, as it is found in calculations (Fig. 3d) only for the pulling configuration (reflecting the experimental case), and not in the planar arrangement.

The rather low ribbon conductance at small bias voltages might seem surprising at first glance, because electronic Tamm states are present close to the Fermi level. However, for the long ribbons

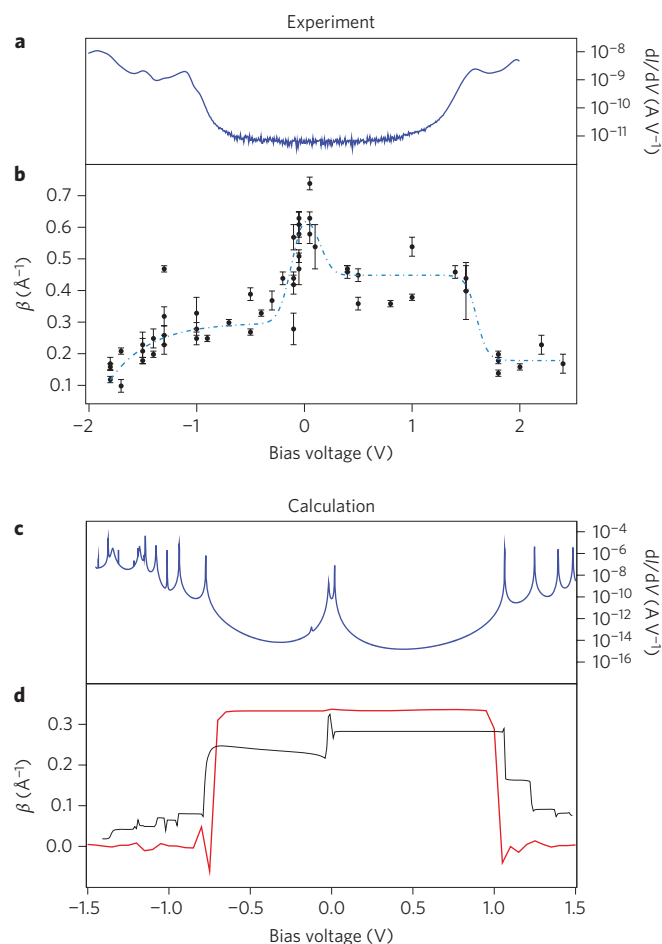


Figure 3 | Charge transport for different electron energies and molecular structures. **a-d**, Conductance dI/dV spectra (**a** and **c**; all in a pulling geometry) of a graphene nanoribbon and its inverse decay length β (**b** and **d**) for different bias voltages from various nanoribbons used in the experiment (**a,b**) and ESQC calculations (**c,d**). **a**, dI/dV spectrum for a nanoribbon in a pulling geometry (planar adsorption leads to similar results; Supplementary Fig. S15). **b**, Error bars reflect the precision in β determination in each individual $I(z)$ curve (at a constant bias voltage and contributing as one data point); a dashed line is drawn to guide the eye. The experimental β values, determined from many nanoribbons, need to be reduced (by $\sim 10\text{--}15\%$) to obtain the real values, because the STM tip height is slightly smaller than the effective molecular length in the junction (Supplementary Fig. S8). **c**, The calculated dI/dV curve (in a pulling geometry) shows the Tamm states resonance doublet, split due to the nanoribbon curvature during pulling. **d**, The ideal planar β curve (red) is presented for comparison with the curve in an STM pulling geometry (black).

considered in this work, there is no overlap of the two Tamm states located at opposite nanoribbon termini, and they do not contribute to the conductance. Calculations for an ideal planar configuration (curve I in Fig. 4a) show exactly this behaviour, with a constant electronic transparency for very short nanoribbons and an exponential decrease for long ones, resulting in a spatial extension of $\sim 1.8 \text{ nm}$ for each Tamm state. This effect was not observed experimentally, because such short nanoribbons were not fabricated (Supplementary Fig. S11).

For a better understanding of the charge transport, we compare in the following the calculated conductance for different ribbon structures and configurations. In comparison to the armchair edge structure at the sides of the nanoribbons in our experiments, a zigzag edge structure strongly improves the conductance. In such

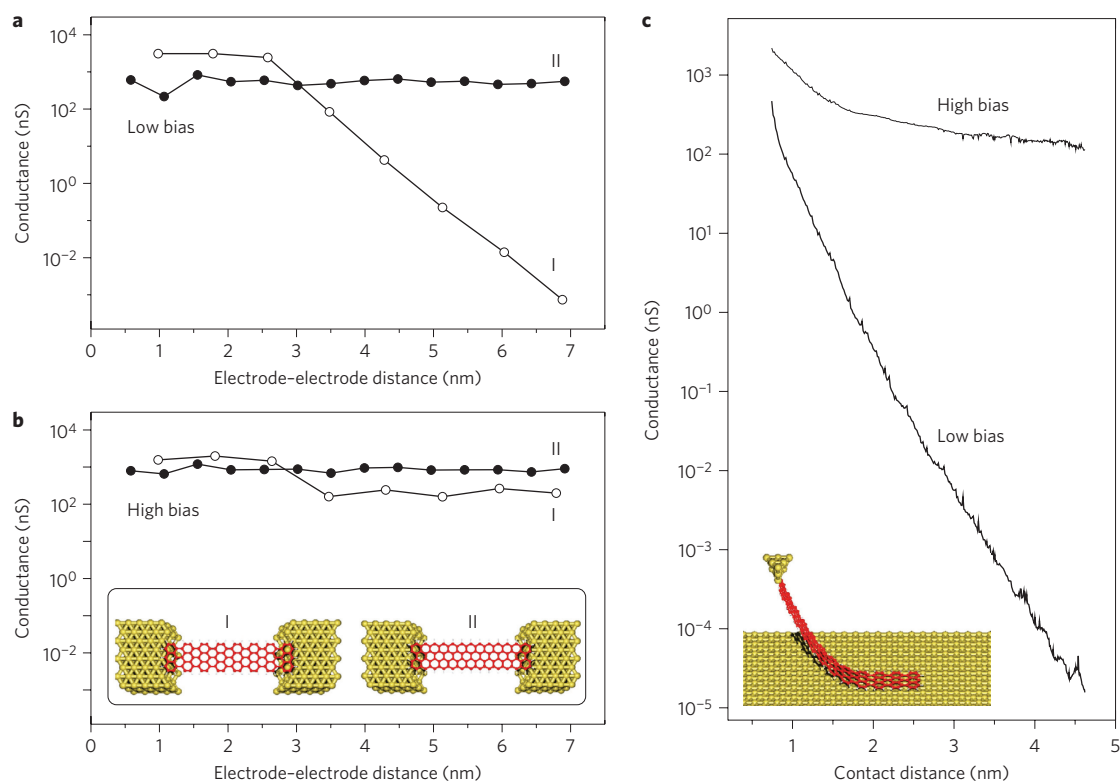


Figure 4 | Calculated conductance for different cases. a, b, Low bias voltage (-0.5 V) in the gap (**a**) and high bias voltage (**b**, -1.0 V; thus matching the HOMO level) for ribbons of different lengths (keeping the same adsorption geometries at the electrode contacts in all cases) either with armchair (I) or zigzag (II) edges sideways (see inset in **b**) in a planar geometry between two electrodes. **c,** Conductance of a 5 nm ribbon with armchair edges in an STM pulling configuration (see inset) as a function of contact distance (that is, the real effective molecular length in the junction; low bias, -0.5 V; high bias, -1.2 V; corresponding regimes are presented in Fig. 3d). The high bias curve first decays significantly (up to a contact distance of ~ 1.5 nm), because the Tamm state contribution is captured at this stage, but at larger contact distances the curvature of the ribbon in the junction still causes a weak decay of the conductance.

a case (curve II in Fig. 4a), the Tamm states are located sideways along the nanoribbon backbone, leading to electronic delocalization along the ribbon and therefore no decay with electrode distance, in agreement with equation (1); in other words, this is pseudo-ballistic transport, because these states are close to the Fermi level. The precise atomic structure therefore has a profound influence on the molecular conductance. Note that there is no strategy as yet to efficiently form such ribbons with zigzag edges sideways in a bottom-up manner. If high bias voltages are applied (Fig. 4b), the dependence on the edge structure essentially vanishes, because efficient transport through the delocalized molecular states takes place.

It is important to note that exponential decay is present in all experimental $I(z)$ curves, even at large bias voltages, when reaching the molecular orbitals (linear slope in Fig. 2b), and efficient (pseudo-ballistic) electron transport takes place only for a planar ribbon where β reaches zero (red curve in Fig. 3d). Our calculations (Fig. 4) show that this is due to the non-planar configuration of the ribbon during the pulling process, because such a deformation modifies the electronic structure and perturbs the electronic delocalization along the molecule (Supplementary Fig. S14), thus reducing convergence towards equation (1), which is based on a perfect regular ribbon structure. Hence, when matching the molecular levels, electron transport is pseudo-ballistic ($\beta = 0 \text{ \AA}^{-1}$) only for an ideal planar ribbon (flat curve I in Fig. 4b), and not if the ribbon is bent (high bias curve in Fig. 4c), as the conductance decays with the molecular length in the junction. Consequently, β values of $\sim 0.1 \text{ \AA}^{-1}$ are calculated in this range (Fig. 3d), in good agreement with the experimental values of between 0.1 and 0.2 \AA^{-1} obtained at high bias voltages (Fig. 3b).

Our results reveal the conductance properties of single graphene nanoribbons and associate them with the atomic structure and electronic states of the ribbons. Various electronic states are identified, and the states for armchair nanoribbons with zigzag end terminations are determined and spatially mapped, and are in very good agreement with calculations. It is found that high conductance values can be reached when approaching the delocalized HOMO and LUMO levels of the molecules with the electron energy. However, it is important to ensure an aromatic system with a planar geometry, because molecular bending—as in the experimental set-up—slightly reduces the conductance, as demonstrated by our calculations. They further reveal that efficient charge transport at low electron energies requires edges with delocalized states close to the Fermi level along the ribbon axis, so sideways zigzag edges are desired for the graphene nanoribbons in the pseudo-ballistic regime, but armchair edges are preferred in the tunnelling regime. We expect that the conductance of such systems can be controlled efficiently via the edge structure, either in a bottom-up on-surface polymerization process or via the substrate, because graphene flakes prefer armchair edges after growth on SiC surfaces²⁹, but zigzag edges on metal surfaces³⁰.

Methods

Experiments were carried out under ultrahigh-vacuum conditions with a base pressure of 10^{-10} mbar. Before depositing the molecules, the Au(111) sample was cleaned by neon ion sputtering ($E = 1.5$ keV) and subsequent annealing to 750 K. A Knudsen cell at a thermocouple-controlled temperature of ~ 470 K was used to evaporate the 10,10'-dibromo-9,9'-bianthryl (DBDA) molecules. The sample was typically held at 470 K during deposition (deposition at room temperature results in single molecules), and the bromine dissociated and anthracene oligomers were

produced (Supplementary Fig. S3) via an on-surface polymerization process by dehalogenation²². Further annealing the Au(111) sample for 5 min to 670 K initiated cyclodehydrogenation²⁴, and fully aromatic graphene nanoribbons were created. A modified commercial low-temperature STM (Createc) was used, and all measurements were taken at ~10 K. The bias, applied to the sample while the tip was grounded, was varied between -1.5 V and +1.6 V in the STM images (constant-current mode). Negative voltages in the dI/dV measurements correspond to occupied states and positive voltages to unoccupied states. Tunnelling spectroscopy was carried out with a lock-in amplifier (frequency = 610 Hz and amplitude = 20 mV), and conductance maps were obtained in constant-current mode. The tip quality was checked via the characteristic appearance of the surface state on clean gold areas. The molecules were purchased from Ruiyuan Group.

Received 5 January 2012; accepted 3 September 2012; published online 14 October 2012; corrected online 19 October 2012

References

1. Tao, N. J. Electron transport in molecular junctions. *Nature Nanotech.* **1**, 173–181 (2006).
2. Weiss, E. A., Wasielewski, M. R. & Ratner, M. A. Molecules as wires: molecule-assisted movement of charge and energy. *Top. Curr. Chem.* **257**, 103–133 (2005).
3. Gray, H. B. & Winkler, J. R. Electron transfer in proteins. *Annu. Rev. Biochem.* **65**, 537–561 (1996).
4. Joachim, C. & Ratner, M. A. Molecular electronics: some views on transport junctions and beyond. *Proc. Natl Acad. Sci. USA* **102**, 8801–8808 (2005).
5. Launay, J.-P. Long-distance intervalence electron transfer. *Chem. Soc. Rev.* **30**, 386–397 (2001).
6. Yamada, R., Kumazawa, H., Noutoshi, T., Tanaka, S. & Tada, H. Electrical conductance of oligothiophene molecular wires. *Nano Lett.* **8**, 1237–1240 (2008).
7. Choi, S. H., Kim, B. & Frisbie, C. D. Electrical resistance of long conjugated molecular wires. *Science* **320**, 1482–1486 (2008).
8. Sedghi, G. *et al.* Long-range electron tunnelling in oligo-porphyrin molecular wires. *Nature Nanotech.* **6**, 517–523 (2011).
9. Temirov, R., Lassise, A., Anders, F. B. & Tautz, F. S. Kondo effect by controlled cleavage of a single-molecule contact. *Nanotechnology* **19**, 065401 (2008).
10. Lafferentz, L. *et al.* Conductance of a single conjugated polymer as a continuous function of its length. *Science* **323**, 1193–1197 (2009).
11. Wang, W., Lee, T. & Reed, M. A. Mechanism of electron conduction in self-assembled alkanethiol monolayer devices. *Phys. Rev. B* **68**, 035416 (2003).
12. Landau, A., Kronik, L. & Nitzan, A. Cooperative effects in molecular conduction. *J. Comp. Theor. Nanosci.* **5**, 535–544 (2008).
13. Joachim, C. & Magoga, M. The effective mass of an electron when tunneling through a molecular wire. *Chem. Phys.* **281**, 347–352 (2002).
14. Li, X. *et al.* Conductance of single alkanethiols: conduction mechanism and effect of molecule–electrode contacts. *J. Am. Chem. Soc.* **128**, 2135–2141 (2006).
15. Wang, C. *et al.* Oligoene single molecular wires. *J. Am. Chem. Soc.* **131**, 15647–15654 (2009).
16. Joachim, C. & Ratner, M. A. Molecular wires: guiding the super-exchange interactions between two electrodes. *Nanotechnology* **15**, 1065–1075 (2004).
17. Han, M. Y., Özyilmaz, B., Zhang, Y. & Kim, P. Energy band-gap engineering of graphene nanoribbons. *Phys. Rev. Lett.* **98**, 206805 (2007).
18. Brey, L. & Fertig, H. A. Electronic states of graphene nanoribbons studied with the Dirac equation. *Phys. Rev. B* **73**, 235411 (2006).
19. Jiao, L., Zhang, L., Wang, X., Diankov, G. & Dai, H. Narrow graphene nanoribbons from carbon nanotubes. *Nature* **458**, 877–880 (2009).
20. Fasoli, A., Colli, A., Lombardo, A. & Ferrari, A. C. Fabrication of graphene nanoribbons via nanowire lithography. *Phys. Status Solidi B* **246**, 2514–2517 (2009).
21. Moreno-Moreno, M., Castellanos-Gomez, A., Rubio-Bollinger, G., Gomez-Herrero, J. & Agrait, N. Ultralong natural graphene nanoribbons and their electrical conductivity. *Small* **5**, 924–927 (2009).
22. Grill, L. *et al.* Nano-architectures by covalent assembly of molecular building blocks. *Nature Nanotech.* **2**, 687–691 (2007).
23. Evaldsson, M., Zozoulenko, I. V., Xu, H. & Heinzel, T. Edge-disorder-induced Anderson localization and conduction gap in graphene nanoribbons. *Phys. Rev. B* **78**, 161407 (2008).
24. Cai, J. *et al.* Atomically precise bottom-up fabrication of graphene nanoribbons. *Nature* **466**, 470–473 (2010).
25. Repp, J., Meyer, G., Stojkovic, S., Gourdon, A. & Joachim, C. Molecules on insulating films: scanning tunneling microscopy imaging of individual molecular orbitals. *Phys. Rev. Lett.* **94**, 026803 (2005).
26. Tamm, I. Über eine mögliche Art der Elektronenbindung. *Phys. Z. Sowjetunion* **1**, 733–746 (1932).
27. Nakada, K., Fujita, M., Dresselhaus, G. & Dresselhaus, M. S. Edge state in graphene ribbons: nanometer size effect and edge shape dependence. *Phys. Rev. B* **54**, 17954–17961 (1996).
28. Tao, C. *et al.* Spatially resolving edge states of chiral graphene nanoribbons. *Nature Phys.* **7**, 616–620 (2011).
29. Rutter, G. M., Guisinger, N. P., Crain, J. N., First, P. N. & Stroscio, J. A. Edge structure of epitaxial graphene islands. *Phys. Rev. B* **81**, 245408 (2010).
30. Tian, J., Cao, H., Wu, W., Yu, Q. & Chen, Y. P. Direct imaging of graphene edges: atomic structure and electronic scattering. *Nano Lett.* **11**, 3663–3668 (2011).

Acknowledgements

The authors acknowledge financial support from European Projects ARTIST and AtMol and the German Science Foundation DFG (through SFB 658). We also acknowledge the A*STAR Computational Resource Centre (A*CRC) for the computational resources and support.

Author contributions

M.K. performed the experiments. M.K. and L.G. analysed the data. F.A. and C.J. carried out the theoretical calculations. L.G. conceived the experiments. L.G. and C.J. wrote the paper. All authors discussed the results and commented on the manuscript.

Additional information

Supplementary information is available in the online version of the paper. Reprints and permission information is available online at <http://www.nature.com/reprints>. Correspondence and requests for materials should be addressed to L.G.

Competing financial interests

The authors declare no competing financial interests.

Voltage-dependent conductance of a single graphene nanoribbon

Matthias Koch, Francisco Ample, Christian Joachim and Leonhard Grill

Nature Nanotechnology <http://dx.doi.org/10.1038/nnano.2012.169> (2012); published online 14 October 2012; corrected online 19 October 2012.

In the version of this Letter originally published online, in the caption for Fig. 1g, the value of the bias voltage was incorrect and should have read -0.55 V. This error has been corrected in all versions of the Letter.